**JM** PAPERS

# Effect of two-way coupling on clustering and settling of heavy particles in homogeneous turbulence

**Roumaissa Hassaini**[1]**, Alec J. Petersen**[2],[†] **and Filippo Coletti**[1]

[1]Department of Mechanical and Process Engineering, ETH Zürich, 8092 Zürich, Switzerland

[2]Department of Civil and Environmental Engineering, University of California Irvine, Irvine, CA 92697, USA

When inertial particles are dispersed in a turbulent flow at sufficiently high concentrations, the continuous and dispersed phases are two-way coupled. Here, we show via laboratory measurements how, as the suspended particles modify the turbulence, their behaviour is also profoundly changed. In particular, we investigate the spatial distribution and motion of sub-Kolmogorov particles falling in homogeneous air turbulence. We focus on the regime considered in Hassaini & Coletti (*J. Fluid Mech.*, vol. 949, 2022, A30), where the turbulent kinetic energy and dissipation rate were found to increase as the particle volume fraction increases from $10^{-6}$ to $5 \times 10^{-5}$. This leads to strong intensification of the clustering, encompassing a larger fraction of the particles and over a wider range of scales. The settling rate is approximately doubled over the considered range of concentrations, with particles in large clusters falling even faster. The settling enhancement is due in comparable measure to the predominantly downward fluid velocity at the particle location (attributed to the collective drag effect) and to the larger slip velocity between the particles and the fluid. With increasing loading, the particles become less able to respond to the fluid fluctuations, and the random uncorrelated component of their motion grows. Taken together, the results indicate that the concentrated particles possess an effectively higher Stokes number, which is a consequence of the amplified dissipation induced by two-way coupling. The larger relative velocities and accelerations due to the increased fall speed may have far-reaching consequences for the inter-particle collision probability.

**Key words:** particle/fluid flow

---

† Email address for correspondence: alecjp@uci.edu

## 1. Introduction

In particle-laden turbulent flows, the dispersed and continuous phases can have a significant effect on each other's dynamics. This situation, usually termed two-way coupling, is common and has been the focus of much of the recent research in the field (Poelma & Ooms 2006; Balachandar & Eaton 2010; Kuerten 2016). Indeed, the portion of the parameter space where the dynamics can be considered one-way coupled is limited: the particle size $d_p$ will be smaller than the Kolmogorov scale $\eta$, and the solid volume fraction $\phi_V$ and mass fraction $\phi_m$ will be below threshold levels for highly dilute suspensions (Brandt & Coletti 2022). The drift due to gravitational acceleration or other body forces will also be relatively small, such that the particle Reynolds number $Re_p$ (based on the particle size and its slip velocity relative to the fluid) does not result in sizeable wakes. The above conditions are rarely met when the particle-to-fluid density ratio $\rho_p/\rho_f$ is of solid–gas mixtures, especially in terrestrial gravity. Usually, two-way coupling has been defined by and investigated for the back-reaction of the particles onto the fluid flow (Hwang & Eaton 2006; Tanaka & Eaton 2010; Zhao, Andersson & Gillissen 2013; Richter & Sullivan 2014; Saito, Watanabe & Gotoh 2019; Hassaini & Coletti 2022). However, the mutual transfer of momentum and energy between the phases implies that the particle behaviour may also be modified, as compared to a hypothetical one-way coupled system of analogous properties. Such modified behaviour of the particles is the focus of the present study.

Perhaps the two most remarkable behaviours of particles in turbulence, and certainly the ones that have attracted the most attention from researchers, are inertial clustering and modified settling. When the response time of small inertial particles $\tau_p$ is comparable to the Kolmogorov time scale $\tau_\eta$ (i.e. when the Stokes number $St_\eta = \tau_p/\tau_\eta$ is of order unity), their instantaneous spatial distribution becomes highly non-homogeneous (Wang & Maxey 1993; Eaton & Fessler 1994; Monchaux, Bourgoin & Cartellier 2012). The resulting clusters exhibit a range of spatial and temporal scales (Yoshimoto & Goto 2007; Gustavsson & Mehlig 2016; Baker *et al.* 2017; Liu *et al.* 2020). The mechanistic origin of clusters, ascribed originally to the centrifuging action of turbulent vortices (Squires & Eaton 1991*b*), remains debated and is likely dependent on the specific combination of parameters (Goto & Vassilicos 2008; Bragg & Collins 2014; Brandt & Coletti 2022). When two-way coupling is at play, the phenomenon can be transformed at various levels. Gualtieri *et al.* (2013) considered homogeneous shear turbulence laden with inertial point-particles at concentrations sufficient to produce two-way coupling. They found that the clusters were more isotropic and smeared compared to their one-way coupled counterparts. Uhlmann & Chouippe (2017) considered homogeneous isotropic turbulence laden with particles larger than the Kolmogorov scales. These modified the local flow field, and their mild tendency to cluster was not associated with intense vortices. Capecelatro, Desjardins & Fox (2018) analysed particle-laden vertical channel flows over a wide range of concentrations. They observed how, at large enough mass loadings, clusters were not caused by shear-driven turbulence, but rather emerged from a regime in which energy dissipation is due to inter-phase drag, similar to cluster-induced turbulence (Capecelatro, Desjardins & Fox 2014).

Particle-laden turbulent flows are also known to display significant alterations of the gravitational settling rate, with respect to the academic case of a particle falling in quiescent fluid (whose terminal velocity equals $\tau_p g$, with $g$ the gravitational acceleration). Already in one-way coupled regimes, multiple mechanisms may either increase or decrease the average vertical velocity (Nielsen 1993; Wang & Maxey 1993; Aliseda *et al.* 2002; Good *et al.* 2014; Petersen, Baker & Coletti 2019). The most commonly

observed mechanism is the preferential sweeping of the particles by downward gusts. The mechanism is revealed by the correlation between particle position and downward fluid velocity fluctuations, as theorized by Maxey (1987), observed numerically by Wang & Maxey (1993), and measured experimentally by Petersen *et al.* (2019). Under two-way coupled regimes, the particle fall speed is usually found to be augmented further. Bosse, Kleiser & Meiburg (2006) attributed the enhanced settling to a collective action of the particles dragging the surrounding fluid downwards. Monchaux & Dejoan (2017) confirmed this view, and additionally reported that two-way coupling disrupted preferential concentration in high-strain regions and so preferential sweeping; thus its role in determining the settling rate was considered marginal. Tom, Carbone & Bragg (2022), on the other hand, while recognizing the collective drag effect of the particles on the fluid, argued that preferential sweeping remained the main mechanism of settling enhancement, but on coarse-grained scales. They interpreted the weaker correlation between particle position and high-strain regions in light of the crossing trajectories effect, by which a fast-falling dispersed phase decorrelates from the local fluid flow (Csanady 1963; Wang & Stock 1993; Berk & Coletti 2021).

The majority of the above-mentioned studies used numerical simulations. The classic point-particle approach has been the most commonly adopted, in which the particles are treated as material points exchanging momentum with the fluid according to simplified expressions for the inter-phase forces. Various issues are associated with this method, including the back-projection of the forces on the computational grid and the definition of the undisturbed fluid velocity in classic drag formulations (Eaton 2009; Balachandar & Eaton 2010; Brandt & Coletti 2022). Advanced strategies, introduced in the last decade to alleviate these issues, lead to better agreement with observations and higher fidelity simulations (Capecelatro & Desjardins 2013; Gualtieri *et al.* 2015; Horwitz & Mani 2016; Ireland & Desjardins 2017; Balachandar, Liu & Lakhote 2019). Moreover, the role of effects usually neglected for small particles, such as torque and lift, has proven to be significant (Andersson, Zhao & Barri 2012; Costa, Brandt & Picano 2020). One-to-one quantitative comparisons with experiments demonstrate the need for continuous improvements (Eaton 2009; Wang *et al.* 2019). Particle-resolved simulations, on the other hand, capture the details of the inter-phase exchanges without modelling the fluid dynamic forces (Tenneti & Subramaniam 2014). The tremendous increase in high-performance computing in recent years enables the application of this method to increasingly large numbers of particles and Reynolds numbers, leading to valuable insights (see, among many others, Lucci, Ferrante & Elghobashi 2010; Garcia-Villalba, Kidanemariam & Uhlmann 2012; Cisse, Homann & Bec 2013; Uhlmann & Doychev 2014; Fornari, Picano & Brandt 2016; Lin *et al.* 2017; Schneiders, Meinke & Schröder 2017; Uhlmann & Chouippe 2017; Mehrabadi *et al.* 2018). The calculations, however, become exceedingly expensive for decreasing particle sizes and increasing $Re_p$. Thus systems featuring sub-Kolmogorov solid particles in air, such as the one considered in the present study, remain out of reach for high-Reynolds-number flows.

Recently, we presented an experimental study of microscopic particles settling in homogeneous air turbulence, in which the loading was varied systematically in the range $\phi_V = 10^{-6} - 5 \times 10^{-5}$ (Hassaini & Coletti 2022). Unlike previous studies focused on massively inertial particles, we observed the turbulent kinetic energy to increase greatly with particle loading, being more than doubled at the highest concentrations. We attributed this behaviour to the potential energy released by the particles into the fluid, also increasing the turbulent dissipation rate. The energy was distributed more homogeneously across the scales compared to unladen turbulence, which was associated with the enhancement of

the inter-scale energy transfer. As the attention was directed entirely on the carrier phase, we did not analyse the behaviour of the dispersed phase. Here, we focus on the spatial distribution and motion of the particles in these experiments, revealing the dramatic impact of two-way coupling on the intensity of clustering and on the settling rate. The paper is organized as follows. Section 2 describes the experimental methodology. Section 3 presents the results in terms of particle spatial distribution (§ 3.1) and motion (§ 3.2). And § 4 summarizes the findings and draws conclusions.

## 2. Experimental methodology

The experiments are carried out in a zero-mean-flow facility described extensively and characterized in Carter *et al.* (2016) and Carter & Coletti (2017, 2018). Briefly, this consists of a 5 m$^3$ chamber where randomly actuated jets generate a region of homogeneous air turbulence, whose intensity is adjusted by varying the firing time of the jets. It was utilized to investigate particle-laden turbulence in Petersen *et al.* (2019), Berk & Coletti (2021) and Hassaini & Coletti (2022). Here, glass micro-spheres (density $\rho_p = 2500$ kg m$^{-3}$) are released at controlled rates via an adjustable hourglass, and enter the chamber after falling through a 3 m chute connected to its ceiling. As quantified in the above-mentioned studies, the apparatus possesses features that make it especially suitable to investigate the interaction of heavy particles with homogeneous turbulence. The region of quasi-homogeneous turbulence at the centre of the chamber is several times larger than the integral scale, which is $O(0.1\,\text{m})$, with small mean velocity (especially in the vertical direction) and weak mean velocity gradients. The turbulence can be forced to Reynolds numbers sufficient to develop a self-similar cascade in the sense of Kolmogorov (1941). The considered particles reach terminal velocity well before entering the chamber and spreading in the homogeneous turbulence region, where they display homogeneous statistics over scales larger than the integral scale (Petersen *et al.* 2019).

The experimental conditions were reported in Hassaini & Coletti (2022) and are summarized briefly here. Two particle diameters are considered, $d_p = 32$ and $52\,\mu\text{m}$, falling in air turbulence at Taylor micro-scale Reynolds numbers $Re_\lambda = 152$ and 289, respectively. These result in Stokes numbers $St_\eta = 0.3$ and 2.6, and comparable settling velocity parameter $Sv_\eta = \tau_p g / u_\eta \approx 3$ in both cases. The simultaneous variation of $Re_\lambda$ and $St_\eta$ is a consequence of working under fixed gravity. As both these parameters are expected to influence the clustering and settling dynamics (Sumbekova *et al.* 2017; Tom & Bragg 2019), isolating their respective effects is not trivial. As both cases show similar behaviours, the comparison indicates that the conclusions that we will draw hold over the present range of parameters. The volume fraction and mass fraction are varied to span the transition from one-way coupling to two-way coupling (Balachandar & Eaton 2010; Brandt & Coletti 2022). For $St_\eta = 0.3$, five cases between $\Phi_v = 10^{-6}$ and $\Phi_v = 4 \times 10^{-5}$ are considered, while for $St_\eta = 0.3$, six cases between $\Phi_v = 10^{-6}$ and $\Phi_v = 5 \times 10^{-5}$ are considered. At these volume fractions, the interparticle distance is larger than $10d_p$ even considering the increase in concentration within clusters (Petersen *et al.* 2019). Therefore, hydrodynamic interactions between particles are deemed negligible. Table 1 summarizes the flow conditions, where the unladen turbulence properties are used as baseline. In table 2, we report the normalized turbulent kinetic energy (TKE) and the large-scale anisotropy ratio over the considered range of particle loading. The turbulence modification by the particles, in particular the substantial increase of TKE, is addressed in detail in Hassaini & Coletti (2022). The analysis conducted in that study, based on an energy budget inspired by Hwang & Eaton (2006), indicated that the increase in TKE is rooted in the

| $d_p$ ($\mu$m) | $\tau_p$ (ms) | $Re_p$ | $St_\eta$ | $Sv_\eta$ | $u'_1$ (m s$^{-1}$) | $u'_1/u'_3$ | $L_{1,1}$ (mm) | $\eta$ (mm) | $Re_\lambda$ | $\phi_{V,max}$ | $\phi_{m,max}$ |
|---|---|---|---|---|---|---|---|---|---|---|---|
| 32 | 7.4 | 0.15 | 0.3 | 2.8 | 0.15 | 1.16 | 79 | 0.58 | 152 | $4 \times 10^{-5}$ | $8.4 \times 10^{-2}$ |
| 52 | 17 | 0.56 | 2.6 | 3.5 | 0.39 | 1.21 | 120 | 0.31 | 289 | $5 \times 10^{-5}$ | $1.5 \times 10^{-1}$ |

Table 1. Particle properties and turbulence statistics (for the unladen flow case) for both investigated configurations. Here, $d_p$ and $\tau_p$ are the particle diameter and response time (calculated using the Schiller–Naumann correlation; see Clift, Grace & Weber 2005); $Re_p$ is the particle Reynolds number based on the still-air terminal velocity; $St_\eta$ and $Sv_\eta$ are the Stokes number and settling velocity parameter based on Kolmogorov scales; $u'_1$ and $u'_3$ are the r.m.s. fluid velocity fluctuations in the horizontal and vertical directions, respectively; $L_{1,1}$ is the integral scale of the turbulence in the horizontal direction; $\eta$ is the Kolmogorov length scale; $Re_\lambda$ is the Taylor micro-scale Reynolds number of the turbulence; and $\phi_{V,max}$ and $\phi_{m,max}$ are the maximum volume and mass fraction of the particles. The minimum volume and mass loadings in the experiments were $10^{-6}$ and $2 \times 10^{-3}$, respectively.

| $\Phi_v$ | | $1 \times 10^{-6}$ | $4 \times 10^{-6}$ | $1 \times 10^{-5}$ | $2 \times 10^{-5}$ | $4 \times 10^{-5}$ | $5 \times 10^{-5}$ |
|---|---|---|---|---|---|---|---|
| $St_\eta = 0.3$ | TKE/TKE$_{\Phi_v=0}$ | 1.12 | 1.26 | 1.33 | 1.39 | 1.65 | — |
| | $u'_1/u'_3$ | 1.05 | 1.07 | 1.06 | 1.14 | 1.16 | — |
| $St_\eta = 2.6$ | TKE/TKE$_{\Phi_v=0}$ | 1.14 | 1.27 | 1.7 | 1.9 | 2.25 | 2.5 |
| | $u'_1/u'_3$ | 1.1 | 1.16 | 1.12 | 1.17 | 1.36 | 1.38 |

Table 2. The normalized turbulent kinetic energy (TKE) and the large-scale anisotropy ratio over the considered range of particle loadings.

gravitational settling: the particles release their potential energy into the flow, increasing its dissipation rate while not significantly altering its integral time scale. The presence of the particles causes the large-scale eddies to become elongated vertically, and redistribute the energy more homogeneously across the scales compared to the single-phase turbulence. The analysis of the inter-scale energy transfer rate suggested that such redistribution is associated with an enhanced direct cascade. We do not derive specific values of the Kolmogorov scales based on the dissipation rate estimated in the particle-laden turbulence. Those values would imply the validity of a universal sub-range in which the Kolmogorov (1941) theory applies, whereas the small-scale turbulence dynamics is known to be heavily modified by the particles (Tanaka & Eaton 2010; Schneiders *et al.* 2017; Hassaini & Coletti 2022).

The key non-dimensional parameters in the previous numerical and experimental studies, and in the present one, are listed in table 3. The list, which is not meant to be exhaustive, includes studies whose range of parameters is especially relevant to the present work: in those experiments, the particles were negatively buoyant and smaller than or comparable to the Kolmogorov scales, and modified the turbulence measurably, while the simulations used the point-particle approach and included the two-way coupling and gravity. Among the experiments, only Yang & Shy (2005) focused on parameters similar to those in our study, and also found turbulence to be augmented by the particles. They did not, however, characterize the effect of two-way coupling on clustering or settling velocity.

A vertical plane at the centre of the chamber is illuminated by an Nd:YLF laser pulsed at 4 kHz and synchronized with two CMOS cameras. These cover a larger field of view (FOV) that captures the integral scales and the large-scale organization of the particles, and a smaller FOV nested in the larger one, to resolve the Kolmogorov scales

*R. Hassaini, A.J. Petersen and F. Coletti*

| | $Re_\lambda$ | $d_p/\eta$ | $\rho_p/\rho_f$ | $St_\eta$ | $Sv_\eta$ | $\tau_p g/u'$ | $\Phi_v$ |
|---|---|---|---|---|---|---|---|
| **Simulations** | | | | | | | |
| Bosse et al. (2006) | 43 | — | 5000 | 1 | 1 | 3.3 | $1.5 \times 10^{-6}$–$1.5 \times 10^{-4}$ |
| Frankel et al. (2016) | 65 | — | 833–8333 | 0.18–5.1 | 1.8–10.7 | 0.5–1.8 | $1.2 \times 10^{-5}$ |
| Monchaux & Dejoan (2017) | 40 | — | 5000 | 0.36–6 | 0.5–2 | 0.25–1 | $1.5 \times 10^{-5}$–$7 \times 10^{-5}$ |
| Tom et al. (2022) | 31–142 | — | 5000 | 0.3–2 | 0.3–2 | 0.9–9.5 | $1.5 \times 10^{-5}$ |
| Rosa, Pozorski & Wang (2020) | 95–121 | — | 833 | 0.25–2.3 | 1.8–16 | 0.32–3.2 | $5 \times 10^{-5}$–$3 \times 10^{-3}$ |
| **Experiments** | | | | | | | |
| Yang & Shy (2005) | 73–202 | 0.03–0.12 | 2080–9420 | 0.4–1.9 | 0.9–6 | 0.1–1.4 | $5 \times 10^{-5}$ |
| Hwang & Eaton (2006) | 230 | 0.96 | 2080 | 58 | 14 | 1.7 | $7 \times 10^{-6}$–$1.4 \times 10^{-4}$ |
| Poelma, Westerweel & Ooms (2007) | 26–29 | 0.4–1.7 | 2.5–3.8 | 0.1–0.5 | 1.3–25 | 0.4–10 | $7 \times 10^{-4}$–$4 \times 10^{-3}$ |
| Tanaka & Eaton (2010) | 127 | 2.3–4.5 | 830–2080 | 138–550 | 7–28 | 1–4 | $5 \times 10^{-5}$–$5 \times 10^{-4}$ |
| Present study | 152–289 | 0.06–0.17 | 2080 | 0.3–2.6 | 2.8–3.5 | 0.4–0.5 | $1 \times 10^{-6}$–$5 \times 10^{-5}$ |

Table 3. Non-dimensional parameters from previous numerical and experimental studies as well as those from the present study.

| | Field of view (mm $\times$ mm) | Resolution (pixel mm$^{-1}$) | PIV vector spacing (mm) |
|---|---|---|---|
| Small FOV | $39 \times 26$ | 33 | 0.36 |
| Large FOV | $128 \times 96$ | 10 | 1.2 |

Table 4. Imaging properties for both fields of view.

and distinguish the closely clustered particles. We will discuss results from both FOVs, whose main imaging parameters are summarized in table 4, as they yield complementary information on the highly multi-scale processes in object. The particle volume fraction is evaluated via direct counting of the particles in the illuminated volume (see Fong, Amili & Coletti (2019), where the approach was validated with a known particle mass loading). A phase-separation algorithm allows us simultaneous characterization of both dispersed phase and carrier phase by particle image velocimetry (PIV) and particle tracking velocimetry (PTV), respectively. The PIV measurements were reported in detail in Hassaini & Coletti (2022); here, we will discuss them inasmuch as they pertain to the particle transport. The PTV measurements follow the same procedure as in Petersen *et al.* (2019) and Berk & Coletti (2021) to locate the particles and reconstruct their trajectories projected on the planar FOV, with a temporal resolution sufficient to obtain velocities and accelerations. To calculate the local slip velocity between fluid and particles, the fluid velocity from the small FOV is evaluated at the particle locations using weighted linear interpolation of the four neighbouring velocity vectors; a comparison with cubic and spline interpolation shows no significant difference (Berk & Coletti 2021). In fact, a linear interpolation is more suitable to evaluate the fluid velocity at the particle location: compared to nonlinear interpolation schemes, this provides a better estimate of the undisturbed fluid velocity at the particle location, which in turn defines the slip velocity relevant to the drag force formulation (Horwitz & Mani 2020).

For each considered set of conditions, we analyse 10 independent runs of 43 000 images, i.e. about 500 integral time scales. The dominant source of uncertainty is the finite sample size. Convergence tests show that each run is well converged for all considered observables (as expected, since each image in the large FOV contains $O(10^3)$ particles), while run-to-run variation is larger. In the following, where appropriate, the standard deviation of the various runs will be used to indicate error bars in the plots. For an in-depth discussion of the measurement uncertainties, we refer to the above-mentioned studies that used the same set-up and techniques.

## 3. Results

In the following, $x_1$ indicates the horizontal direction parallel to the jet axes and to the imaging plane, $x_2$ is horizontal and perpendicular to $x_1$, and $x_3$ is vertical and pointing downwards; the respective velocity components are $U_1$, $U_2$ and $U_3$. The fluctuating velocities in the $i$th direction are denoted by $u_i = U_i - \bar{U}_i$, where the overbar indicates spatio-temporal average. Root-mean-square (r.m.s.) fluctuations are indicated with a prime. The subscript $p$ refers to quantities related to the particles, $f$ to the fluid, and $f \,|\, p$ to fluid properties interpolated at the particle location. Throughout the section, for clarity and brevity, we will display selected cases, more often focusing on the $St_\eta = 2.6$ case (which was studied over a somewhat wider range of loadings) and its vertical component of motion; when not specified otherwise, these will be representative of
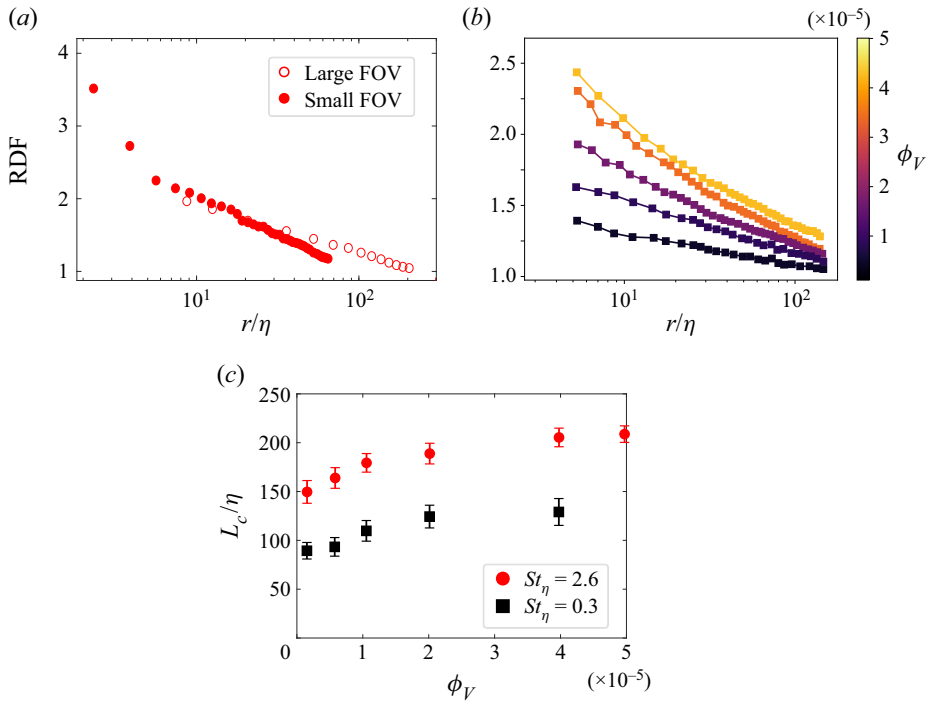
Figure 1. Radial distribution functions (RDFs) for (*a*) both FOVs of the case $St_\eta = 0.3$, $\phi_V = 4 \times 10^{-5}$, and (*b*) the large FOV of the case $St_\eta = 2.6$. (*c*) The characteristic clustering length normalized by the Kolmogorov length scale as a function of volume fraction for the cases $St_\eta = 0.3$ (black squares) and $St_\eta = 2.6$ (red circles).

all considered conditions. Comparisons will be drawn with various previous studies, the majority of which are numerical simulations. Often, such comparisons can be only qualitative, due to differences in the input parameters, in particular $Re_\lambda$. Nevertheless, clear trends will be highlighted that are deemed to depend weakly on the precise set of parameters.

### 3.1. *Particle spatial distribution*

We first consider the radial distribution function (RDF), which describes the scale-by-scale concentration in the area surrounding a generic particle compared to a uniform distribution (Sundaram & Collins 1997). For two-dimensional fields such as those obtained by planar imaging, this is defined as

$$g(r) = (N_r/A_r)/(N_{tot}/A_{tot}), \tag{3.1}$$

where $r$ is the generic inter-particle separation, $N_r$ is the number of particles within an annulus of area $A_r$, and $N_{tot}$ is the total number of particles within the planar domain of area $A_{tot}$. Details of the implementation are described in Petersen *et al.* (2019), including potential sources of bias. In particular, values of $g(r)$ at separations below the illuminated volume thickness ($\sim 6\eta$) are affected by projection biases (Holtzer & Collins 2002). In figure 1(*a*), we plot RDFs from both small and large FOV for the case $St_\eta = 0.3$, $\phi_V = 4 \times 10^{-5}$. For $r/\eta < 5$, the data from the small FOV depart sharply from the exponential decay displayed at larger separation, while for $r/\eta > 8$, the RDFs from both FOVs are in good agreement. We therefore use RDFs from the large FOV to illustrate the effect
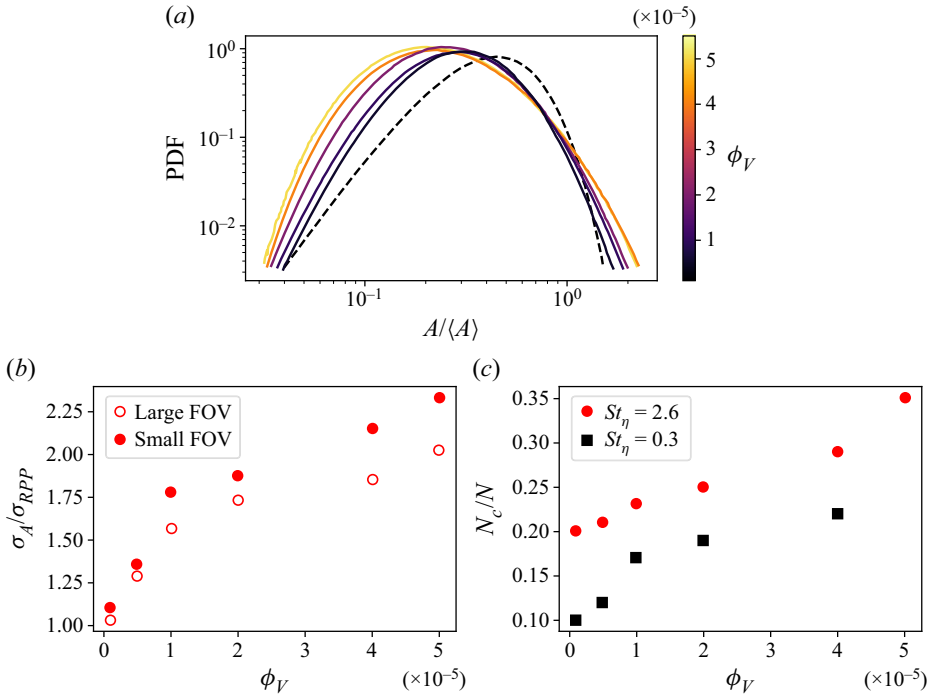
**976** A12-8

Figure 2. (*a*) PDF of the Voronoï cell areas normalized by the mean value for the case $St_\eta = 2.6$, compared to the distribution found in a random spatial distribution (dashed black line). (*b*) Standard deviation of such distributions for the case $St_\eta = 0.3$, with filled and empty symbols indicating small and large FOVs, respectively. (*c*) Fraction of clustered particles for the cases $St_\eta = 0.3$ and 2.6.

of increasing $\phi_V$ for the case $St_\eta = 2.6$ (figure 1*b*), with the case $St_\eta = 0.3$ displaying analogous trends.

As is apparent in figure 1(*b*), with increasing particle loading, clustering is more intense and extends over larger scales. For a quantitative assessment, we consider the classic fit proposed by Reade & Collins (2000):

$$g(r/\eta) = 1 + c_0(r/\eta) - c_1 \exp(-c_2 r/\eta). \tag{3.2}$$

The length scale $L_c = \eta/c_2$ defines the extent of the exponential decay, which dominates the behaviour at large separations (Reade & Collins 2000). Therefore, this is taken as a measure of the scale over which clustering occurs. It is obtained by a least squares fit and shown in figure 1(*c*) as a function of $\phi_V$, displaying an increasing trend for both considered $St_\eta$ values. As expected, the more inertial particles, which respond to larger eddies, cluster over larger scales. This is in keeping with the theoretical work of Goto & Vassilicos (2006) and Yoshimoto & Goto (2007), and with simulations from Bec *et al.* (2010) and Ireland, Bragg & Collins (2016*a*). The difference between the particle types is likely magnified by the effect of gravity, which is expected to enhance clustering for $St_\eta > 1$ and attenuate it for $St_\eta < 1$ (Bec, Homann & Ray 2014; Gustavsson, Vajedi & Mehlig 2014; Ireland, Bragg & Collins 2016*b*; Baker *et al.* 2017).

The particle spatial distribution is characterized further by Voronoï tessellation, in which every particle is inscribed in a polygonal cell whose size represents the inverse of the local concentration (Monchaux, Bourgoin & Cartellier 2010). Figure 2(*a*) shows the probability density functions (PDFs) of the Voronoï cell areas $A$ for the case
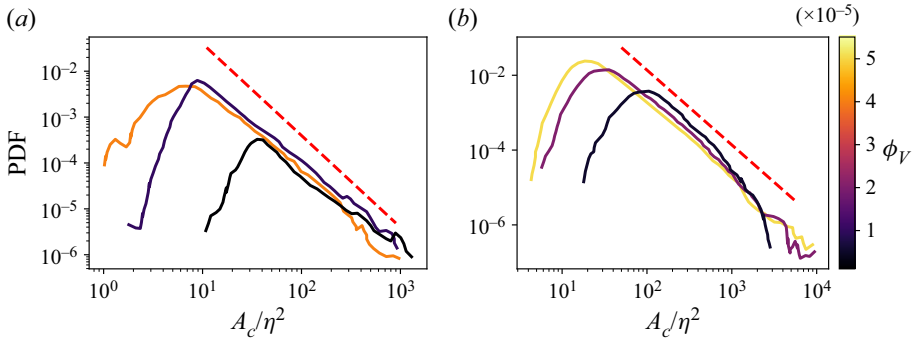
Figure 3. PDFs of the normalized cluster area for the case $St_\eta = 0.3$ in (*a*) the small FOV and (*b*) the large FOV. The dashed lines indicate a $-2$ power-law decay.

$St_\eta = 2.6$ at the various $\phi_V$. The broadening of the distributions, signalling more inhomogeneous concentration fields, confirms that clustering is intensified with increasing volume fraction. This is quantified in figure 2(*b*), where the standard deviation of such distributions, $\sigma_A$, is normalized by the expected value for particles distributed according to a random Poisson process, $\sigma_{RPP} \sim 0.53$ (Monchaux *et al.* 2010). Again, the augmentation of clustering at larger particle loadings is dramatic, and the effect is not significantly dependent on the size of the FOV. The latter, however, influences the quantitative values, because spatial resolution and imaging window size impact the detection of individual particles and clusters. Additionally, this trend is captured by considering the number $N_c$ of particles belonging to individual clusters, compared to the total number of particles $N_{tot}$ imaged in each case (figure 2*c*). Individual clusters are defined by the contiguous set of Voronoï cells smaller than a threshold corresponding to the intersection between observed and random distributions (see Baker *et al.* (2017) and Petersen *et al.* (2019) for details). The ratio $N_c/N_{tot}$ approximately doubles over the considered range of $\phi_V$.

Figures 3(*a*) and 3(*b*) display the PDFs of the cluster area $A_c$ for the case $St_\eta = 0.3$, as captured in the small and large FOVs, respectively. Both views exhibit a power-law behaviour over multiple decades, with a slope close to $-2$ as reported previously (Monchaux 2012; Baker *et al.* 2017; Petersen *et al.* 2019). The small FOV indicates a prevalent cluster area $A_c = 10\eta$–$60\eta$, with a tendency for the size ranges to reach smaller values at higher concentrations. Besides being a consequence of two-way coupling, this is possibly also due to the fact that sparser particle fields can probe only coarser scales – a source of bias in the Voronoï method (Monchaux 2012). Indeed, this tendency is also apparent in the large FOV, where the spatial resolution is lower and the peak of the PDF would suggest clusters twice as large compared to the small FOV. On the other hand, the small FOV imposes a cut-off to the maximum detectable cluster size, while the large FOV allows us to capture the stretching of the power-law distributions to much greater $A_c$. These extend to $O(10^4\eta^2)$ as $\phi_V$ increases, i.e. reaching the integral scales. Combined, the measurements from both FOVs overcome each other's limitations, and indicate that self-similar clusters occur over a range of scales that grows with particle loading.

The observed intensification of clustering at larger volume fractions contrasts with results from previous numerical studies. Monchaux & Dejoan (2017) found that for $St_\eta$ and $Sv_\eta$ comparable to our experiments, clustering as quantified by Voronoï tessellation was less intense with increasing $\phi_V$. In similar regimes, Rosa *et al.* (2022) found that the RDFs evaluated at the particle radius (specifically relevant for collisions) had a
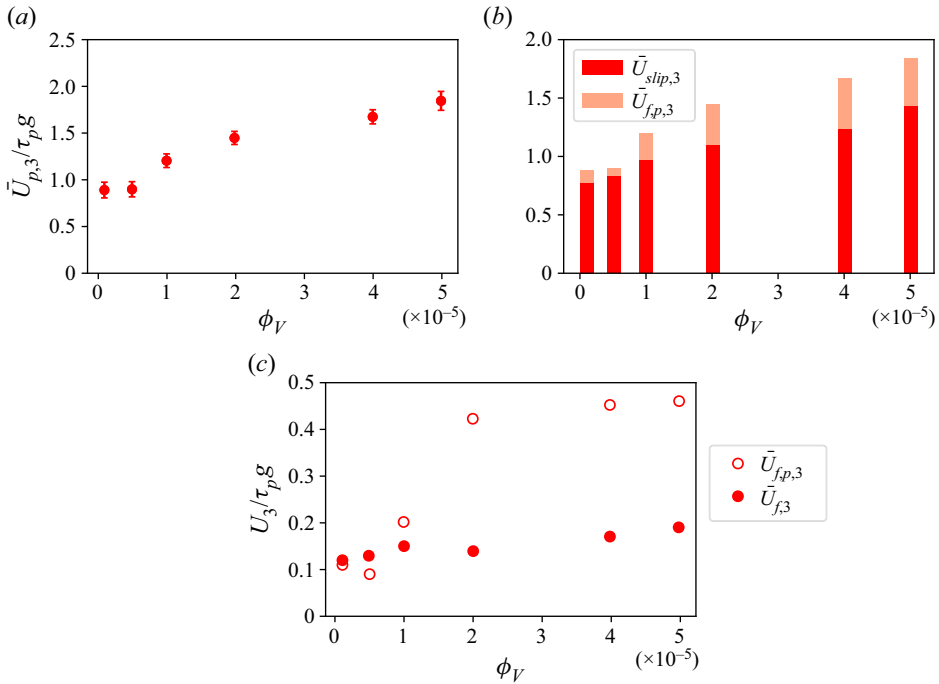
**976** A12-10

Figure 4. (*a*) Mean fall speed of the particles, normalized by the still-air terminal velocity $\tau_p g$, for the case $St_\eta = 2.6$. (*b*) Mean fall speed partitioned between contributions of the vertical slip velocity and the vertical fluid velocity at the particle location. (*c*) Comparison between the mean vertical fluid velocity and the mean vertical fluid velocity at the particle location.

non-monotonic behaviour, first increasing and then decreasing with growing particle concentration. Both simulations used a point-particle approach. The extensive laboratory study from Sumbekova *et al.* (2017) did report a moderate tendency of clustering to be enhanced at higher volume fractions. This, however, was overshadowed by the dominant effect of $Re_\lambda$. Their study featured polydisperse droplets, thus a direct comparison with the present experiments is not straightforward. The physical explanation for the amplified clustering that we observe, and its larger spatial extent at higher loadings, lies in the turbulence modification described in Hassaini & Coletti (2022). We will discuss this point in the following.

### 3.2. *Particle motion*

We first consider the mean vertical velocity of the particles $\bar{U}_{p,3}$ normalized in figure 4(*a*) by the still-air terminal velocity $\tau_p g$. The settling rate increases substantially with volume fraction; for $St_\eta = 2.6$, the vertical velocity doubles over the considered range of loadings. Globally, the settling enhancement is comparable to the numerical simulations of Bosse *et al.* (2006), Monchaux & Dejoan (2017) and Tom *et al.* (2022) over similar ranges of particle inertia and concentration (though at much lower $Re_\lambda$), while Rosa *et al.* (2022) found smaller settling enhancement. To quantify the role of the different mechanisms at play, we consider the slip velocity $U_{slip} = U_p - U_{fp}$, i.e. the particle velocity relative to the surrounding flow. This follows the definition of slip velocity used, e.g. in Berk & Coletti (2021), though the opposite sign convention is also used in the literature. In figure 4(*b*), the
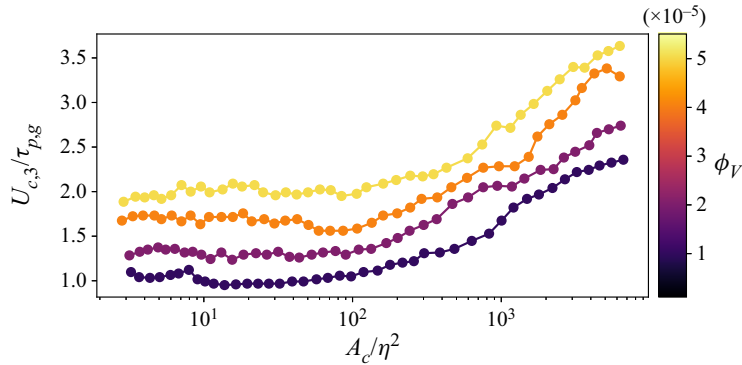
**976** A12-11

Figure 5. Cluster fall speed (normalized by the still-air terminal velocity) as a function of their size, for the case $St_\eta = 2.6$.

mean settling velocity for the case $St_\eta = 2.6$ is thus decomposed as $\bar{U}_{p,3} = \bar{U}_{slip,3} + \bar{U}_{fp,3}$; the case $St_\eta = 0.3$ yields analogous trends. Both terms are seen to grow significantly over the considered range of $\phi_V$. In one-way coupled systems, $\bar{U}_{fp,3}$ encapsulates the contribution of preferential sweeping, while in the presence of two-way coupling, it also includes the effect of the particles dragging the local fluid downwards. Discriminating between the effects is not strictly possible in an experimental setting, where the abstraction of pure one-way coupling cannot be made. We note, however, that in the considered case, preferential sweeping is negligible at the lower loadings (consistent with previous measurements in the same set-up; Petersen *et al.* 2019). Therefore, we speculate that collective drag is the main contributor to $\bar{U}_{fp,3}$ at the higher considered volume fractions, as in Bosse *et al.* (2006) and Monchaux & Dejoan (2017).

Remarkably, the contribution of $\bar{U}_{slip,3}$ to the vertical velocity also grows significantly with $\phi_V$. This is in contrast with the observation by Monchaux & Dejoan (2017) that the local slip velocity tends to vanish at the larger particle loadings. In other studies where settling in quiescent fluids was enhanced by collective drag, the slip velocity was found to remain close to the terminal velocity of an isolated particle. This was the case in the particle-resolved simulations of Uhlmann & Doychev (2014) and in the recent experiments of Zürner *et al.* (2023). In the particle-resolved turbulence simulations of Chouippe & Uhlmann (2019), the vertical slip was slightly smaller than the single-particle terminal velocity, but this was attributed to the tendency of the particles to be in each other's wake, as is typical of their regime ($Re_p = O(10^2)$, two orders of magnitude larger than here). In the present situation, the increase of $\bar{U}_{slip,3}$ is interpreted as a consequence of the amplified turbulent activity at the higher $\phi_V$: the more concentrated dispersed phase excites small-scale turbulent fluctuations (Hassaini & Coletti 2022), whose time scales become shorter; these cannot readily be followed by the inertial particles, causing them to lag further the fluid motion and increasing the instantaneous slip velocity.

In the present regimes, the falling particles do not cause a significant global downward motion of the fluid. This is verified in figure 4(*c*), where $\bar{U}_{slip,3}$ is shown to increase weakly with $\phi_V$, remaining small with respect to all relevant velocity scales of the system. This is important in order to be able to compare our results to numerical simulations, in which $\bar{U}_{slip,3} = 0$ is imposed by a vertical pressure gradient to prevent the kinetic energy from diverging (Bosse *et al.* 2006; Monchaux & Dejoan 2017; Tom *et al.* 2022).
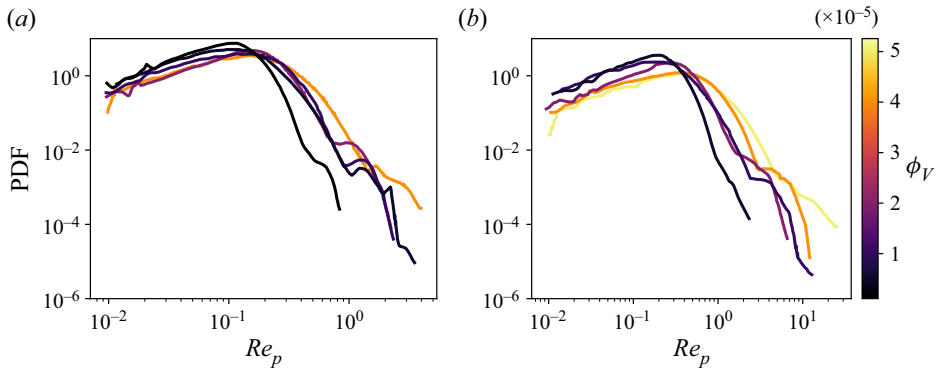
**976** A12-12

Figure 6. PDFs of the particle Reynolds number for the cases (*a*) $St_\eta = 0.3$ and (*b*) $St_\eta = 2.6$.

The substantial increase in settling rate with increasing particle loading applies also to the clusters. In figure 5, we plot the cluster settling velocity $\bar{U}_{c,3}$ for the case $St_\eta = 2.6$, obtained by averaging the vertical velocity of all particles belonging to clusters in a given size range. This is normalized by $\tau_p g$, and plotted against the cluster area $A_c$ (in Kolmogorov units). We observe a substantial increase in settling velocity with cluster size, especially for $A_c > 100\eta^2$. This was noted also in Petersen *et al.* (2019), but the respective roles of collective drag and preferential sweeping could not be clearly discerned. Here, we observe a systematic increase of settling velocity with volume fraction, which suggests that collective effects play an important role over the present range of loading. It is remarkable that the larger clusters at $\phi_V = 5 \times 10^{-5}$ fall almost four times faster than the still-air, single-particle terminal velocity.

Beside the vertical velocity, the slip velocity generally increases with increasing volume fraction. This is shown in figure 6, plotting the PDF of the particle Reynolds number $Re_p = U_{slip} d_p / \nu$ estimated based on the in-plane slip velocity $U_{slip} = \sqrt{U_{slip,1}^2 + U_{slip,3}^2}$. As expected, the values remain well below the vortex-shedding regime. Therefore, the turbulence modification is due to the local enhancement of dissipation around the particles and by their collective action, rather than by the injection of energetic wakes (Hassaini & Coletti 2022). However, with increasing $\phi_V$, one observes a significant probability of $Re_p$ exceeding unity by a wide margin – a situation that complicates the applicability of the point-particle approach. We also remark that $Re_p$ is here underestimated systematically as the out-of-plane velocity component is not measured. Finally, we note that the particle Reynolds numbers based on the terminal velocity ($Re_p = 0.15$ and $0.56$ for the cases $St_\eta = 0.3$ and 2.6, respectively) are similar to the mean of the $Re_p$ distributions based on the slip velocity. Therefore, basing the particle response time on the latter would lead to similar values, as the far tails of the PDF would have limited statistical significance.

So far, we have shown how, at increasing loading, the particles tend to cluster over larger ranges of scales and to slip away more from the local fluid. Both such observations imply that with larger $\phi_V$, the particles become more inertial with respect to the fluid motion, or in other words, that their effective $St_\eta$ becomes larger. The particle response is not expected to change significantly with $\phi_V$, except for slight adjustments due to the increase of $Re_p$ and the consequent correction of $\tau_p$ (see Clift *et al.* 2005). On the other hand, the total turbulent dissipation (which includes the dissipation in the boundary layer around each particle) is approximately doubled over the considered range of volume fractions compared to the single-phase turbulence, as shown in Hassaini & Coletti (2022). By Kolmogorov scaling,
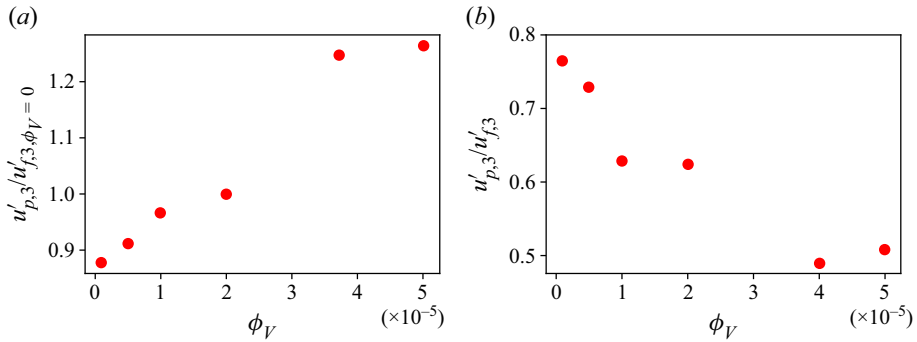
Figure 7. The r.m.s. velocity fluctuations of the particles (*a*) normalized by that of the fluid in the unladen case and (*b*) at the corresponding volume fraction. Data for the case $St_\eta = 2.6$.
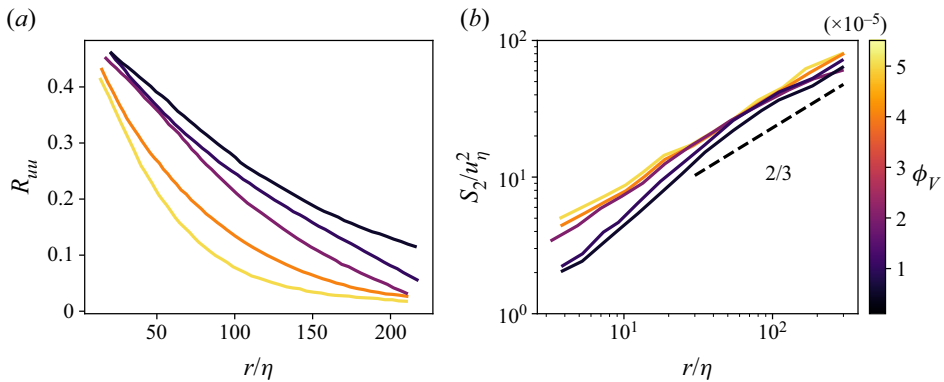


Figure 8. (*a*) Autocorrelation function and (*b*) second-order velocity structure function for the particles in the case $St_\eta = 2.6$.

this produces small-scale motions of shorter time scale, which in turn amplifies the lag between fluid and particles. This view is supported by the following analysis of the particle fluctuating velocity.

In figure 7(*a*), the vertical component of the particle r.m.s. fluctuation, $u'_{p,3}$, is normalized by the fluid counterpart for the unladen case, $u'_{f,30}$. At $\phi_V = O(10^{-6})$, for which the particle dynamics can be considered approximately one-way coupled, the particle fluctuations are slightly weaker than the fluid fluctuations, as expected in this range of $St_\eta$ and $Sv_\eta$ (Good *et al.* 2014). With higher loadings, the particle fluctuating energy grows larger in response to the strong turbulence enhancement caused by the two-way coupling (Hassaini & Coletti 2022). On the other hand, normalizing $u'_{p,3}$ by the fluid fluctuation at the corresponding volume fraction, $u'_{f,3}$, returns the opposite trend. Clearly, the more concentrated particles are less and less capable of responding to the turbulence augmented by their very presence; this is again consistent with the notion that their effective inertia grows at higher loadings. Additionally, the larger settling rate magnifies the decorrelation from the local flow structures, which also contributes to a weaker response of the particles to the fluid fluctuating energy (Wang & Stock 1993; Berk & Coletti 2021).

**976** A12-14

The particle response to the underlying turbulence can be described further by two-point statistics. The Eulerian velocity correlation is plotted in figure 8(*a*), which gives information on the spatial coherence of the particle motion (Fevrier, Simonin & Squires 2005). As in Fong *et al.* (2019), we write it as a correlation coefficient between the longitudinal velocity fluctuations of particles *m* and *n*, separated by a vector *r*, and normalized by the velocity variance:

$$R_{uu}(r) = \frac{\overline{u^m u^n \mid x = x_p^m; \, x + r = x_p^n}}{\overline{u^2}} \tag{3.3}$$

Here, *x* is a spatial location within the FOV, $x_p^i$ is the position of the particle *i*, and the fluctuating velocities are projected along *r*. The coefficient does not approach unity for vanishingly small separations, indicating that a sizeable fraction of the particle velocity is spatially uncorrelated. This 'random uncorrelated motion', rooted in the memory of interactions with distant eddies, represents a larger fraction of the total for more inertial particles (Fevrier *et al.* 2005; Wilkinson & Mehlig 2005; Bragg & Collins 2014; Fong *et al.* 2019). For particles of non-negligible inertia, such a component of the motion is considered among the main causes of small-scale clustering (Gustavsson & Mehlig 2016). Here, the correlation coefficient is lower for higher loading and also decays more rapidly with increasing $\phi_V$. Therefore, despite the clusters stretching over larger scales, the particle motion becomes less spatially coherent. This is further evidence that the particles acquire a larger effective $St_\eta$ at higher loadings.

Similar considerations apply to the relative particle velocity, quantified in figure 8(*b*) by the second-order longitudinal structure function $S_2(r) = \overline{[u(x + r) - u(x)]^2}$, where again we take the components of the fluctuating velocities along the separation vector *r*. We note that the finite thickness of the laser sheet leads to an overestimation of the relative velocity over the separations $r \lesssim 6\eta$ (Dou *et al.* 2018), but this may not overshadow the trend. For tracers, $S_2$ scales as $r^2$ and $r^{2/3}$ in the dissipative and inertial range, respectively (Kolmogorov 1941). For heavy particles, due to the above-mentioned memory effect and lack of spatial correlation, the relative velocities between close particles increase, and $S_2(r)$ progressively deviates from the $r^2$ scaling at small separations; see numerical simulations by Bec *et al.* (2010) and Ireland *et al.* (2016*a,b*), among others, and experimental measurements by Dou *et al.* (2018) and Berk & Coletti (2021). Here, we observe a systematic increase in relative velocity with volume fraction. This is again in line with the notion that the particles have higher $St_\eta$. This in turn may cause higher collision frequency (Sundaram & Collins 1997), though the present measurements do not have sufficient spatio-temporal resolution to quantify such an effect.

Finally, we consider the particle acceleration, whose PDF is plotted in figure 9(*a*). We display the vertical component, the horizontal one behaving similarly. For all considered cases, the mean acceleration is small, as the particles have reached terminal velocity before entering the FOV. The distributions display the familiar exponential tails signalling intermittency, which is, however, modulated by inertial filtering (Ayyalasomayajula *et al.* 2006; Bec *et al.* 2006). Normalizing the acceleration PDF by its r.m.s. fluctuations reduces the spread of the distributions but does not lead to a collapse, unlike in Qureshi *et al.* (2007), where dilute neutrally buoyant particles of varying size were considered. The acceleration variance is presented in figure 9(*b*) for both values of $St_\eta$, as a function of $\phi_V$. The values are normalized by those predicted by the model of Berk & Coletti (2021) (see their (4.12)), who expanded on the theory of Csanady (1963) to derive expressions for the time scale of the flow experienced by heavy particles. At the lowest volume fraction, the measured values agree closely with the theory, which applies to one-way
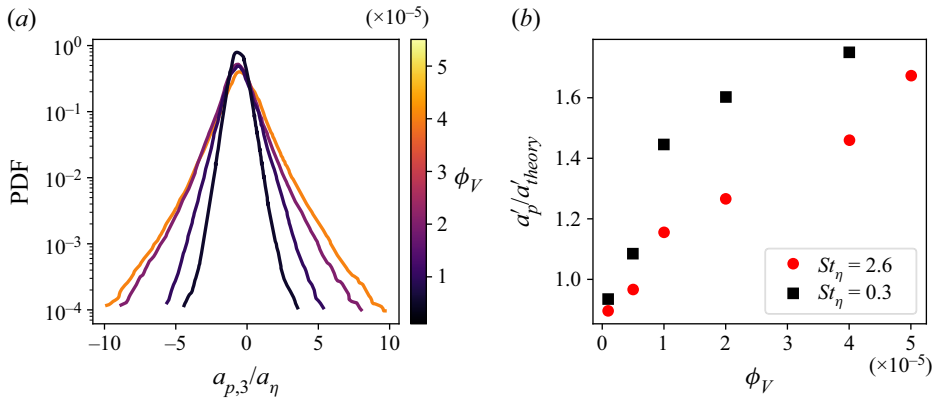
Figure 9. (*a*) PDF of the vertical particle accelerations for the case $St_\eta = 2.6$, normalized by the Kolmogorov acceleration. (*b*) The r.m.s. particle acceleration normalized by the theoretical prediction of Berk & Coletti (2021) for the cases $St_\eta = 0.3$ and 2.6.

coupled systems. With increasing loading, the particles exhibit a substantial increase of acceleration variance. This is seemingly in contrast with the idea that the particles are effectively more inertial in the more concentrated regime, as argued above. The contradiction is resolved by recognizing that the acceleration is dominated by the other major consequence of two-way coupling, namely the settling enhancement. This intensifies the crossing trajectories effect, which causes particles to experience quickly changing flow conditions (Squires & Eaton 1991*a*; Elghobashi & Truesdell 1992; Wang & Stock 1993). Thus, as the particles fall faster, their effective $Sv_\eta$ increases, in turn augmenting their acceleration variance (Ireland *et al.* 2016*b*; Berk & Coletti 2021). In addition to this effect, the enhanced turbulence intensity caused by the particles themselves also contributes to augmenting their acceleration.

## 4. Conclusions

We have analysed the behaviour of heavy particles in homogeneous turbulence, with $St_\eta$ and $Sv_\eta$ of order unity, increasing the volume fraction systematically from $\phi_V = 10^{-6}$ to $\phi_V = 5 \times 10^{-5}$ to isolate the effect of two-way coupling on the spatial organization and motion of the dispersed phase. We find that both clustering and settling are strongly enhanced when the loading is increased. In particular, both RDFs and the Voronoï tessellation method show that with increasing $\phi_V$, particle clustering is intensified at all scales. Combining two nested FOVs, we find that the more concentrated particles form self-similar clusters whose size range reaches deeper into the dissipative range and stretches further over the integral scales. The particle settling velocity is approximately doubled over the considered range of volume fractions. This is due, in approximately equal measure, to two factors: an increased association of the particle location with downward fluid velocity, and a larger slip velocity between the particles and the fluid. The former may be caused by both preferential sweeping and collective drag. While we cannot discriminate conclusively between these two effects, the fact that preferential sweeping is not significant in the most dilute regime suggests that collective drag plays a dominant role. The extended scales of the cluster and the increased slip velocity suggest that the particles attain an effectively larger $St_\eta$ as a consequence of the turbulence modification. This is confirmed

**976** A12-16

by the behaviour of the particle fluctuating energy, which becomes a smaller fraction of the turbulent kinetic energy (TKE) as the loading is increased.

These findings can be understood in light of the effect that the particles themselves have on the underlying turbulence, which we investigated recently in Hassaini & Coletti (2022). There, we demonstrated and quantified how the dispersed phase enhances the TKE and its dissipation rate by releasing potential energy into the fluid, exciting in particular the smallest scales of the fluid motion. This yields faster dissipative time scales, which the particles are less able to follow. Indeed, the two-point particle velocity statistics indicate how at higher concentrations, the uncorrelated component of the particle motion becomes larger and comparable to the correlated one. Likewise, the relative particle velocity at small separations increases. This is consequential for the collision probability, although the latter will depend on short-range interactions (Bragg *et al.* 2022) that are not resolved here.

In Hassaini & Coletti (2022), we estimated that the overall dissipation rate was approximately doubled over the present range of particle loading, which would imply an increase of about 40 % of the effective $St_\eta$ and a decrease of about 20 % of $Sv_\eta$. The same study, however, demonstrated how the turbulence is altered in qualitatively different manners at the different scales. Therefore, it is not straightforward to condense the multifaceted changes in particle–turbulence interaction in the value of the effective $St_\eta$ and $Sv_\eta$.

We confirm that $\phi_V = O(10^{-6})$ is a robust threshold for the emergence of two-way coupling (Elghobashi 1994), not only from the standpoint of turbulence modification but also in terms of particle behaviour. This is verified only at the present high density ratios, typical of solid–gas systems; for solid–liquid suspension, a criterion remains to be determined univocally (Brandt & Coletti 2022). Indeed, the threshold is more likely to be determined by the mass fraction $\phi_m$, which governs the momentum transfer. A clear distinction between the effects of $\phi_V$ and $\phi_m$ can be discerned only by changing the solid-to-fluid density ratio, which is outside the scope of our study. In the future, this could be achieved by contrasting, e.g. plastic particles against metallic ones, or resorting to adjustable soap bubbles as in Qureshi *et al.* (2008).

The increase of the effective $St_\eta$ alone does not explain the increase in $\bar{U}_{slip,3}$. Clearly, gravity breaks the symmetry in the distribution of the vertical slip velocity $U_{slip,3}$ as it does for $U_{fp,3}$: both have non-zero mean whose magnitude increases with volume fraction. Tom *et al.* (2022) found in their numerical simulations that heavy particles are often found in high-strain regions of the velocity field coarse-grained at scales corresponding to the particle response time. This was proposed as a spatially filtered version of preferential sweeping: the particles are swept downwards by eddies more energetic than the Kolmogorov-size vortices. According to this view, preferential sweeping (here promoted by two-way coupling) may play a role in the increase of downward slip velocity with volume fraction: the more energetic eddies sweeping down the particles may lead to larger slip velocities, as we observe. As the particles take a finite time to adjust to the local flow conditions, this can result in globally enhanced settling velocities.

The present findings provide indications for the mechanistic interpretation of the complex particle-turbulence interplay, also in regard to aspects that have remained elusive, such as the origin of clustering (Brandt & Coletti 2022). In this regard, we note how, while the trends for both considered particle sizes are similar, clustering is more intense for $St_\eta > 1$. This does not support the notion that particle accumulation is driven mainly by the centrifuging mechanism; this applies strictly for $St \ll 1$, and under relatively weak gravitational drift (Maxey 1987). Mechanisms that can account for significant inertia

and crossing trajectories are more likely to cause the observed trends. In particular, the path-history effect (Bragg & Collins 2014) is consistent with our observations, especially considering the association of clustering with the uncorrelated motion of the dispersed phase.

These results can also inform numerical models with various degrees of fidelity, as it is possible presently to realize two-way coupled point-particle simulations in the considered range of $Re_\lambda$ and $\phi_V$. Of particular interest is the fact that the increase of $\phi_V$ is associated to a significant probability of $Re_p$ exceeding unity by a wide margin – a situation for which the applicability of the point-particle approach needs to be tested systematically. Finally, we note that the planar imaging technique adopted here has allowed for relatively high concentrations, which would have been challenging to achieve with classic reconstruction algorithms for volumetric imaging. Recent advances in three-dimensional Lagrangian particle tracking, however, allow for accurate measurements at comparably dense concentrations (Discetti & Coletti 2018; Schröder & Schanz 2023). Their application in the considered regimes is warranted, as this would reveal the effect of two-way coupling on other relevant observables, such as the Lagrangian dispersion (Bourgoin 2015) and the lifetime of clusters (Liu *et al.* 2020).

**Declaration of interests.** The authors report no conflict of interest.

**Author ORCIDs.**

Ⓓ Roumaissa Hassaini https://orcid.org/0000-0003-4501-5305;

Ⓓ Alec J. Petersen https://orcid.org/0000-0001-5480-458X;

Ⓓ Filippo Coletti https://orcid.org/0000-0001-5344-2476.

REFERENCES

ALISEDA, A., CARTELLIER, A., HAINAUX, F. & LASHERASH, J.C. 2002 Effect of preferential concentration on the settling velocity of heavy particles in homogeneous isotropic turbulence. *J. Fluid Mech.* **468**, 77–105.

ANDERSSON, H.I., ZHAO, L. & BARRI, M. 2012 Torque-coupling and particle–turbulence interactions. *J. Fluid Mech.* **696**, 319–329.

AYYALASOMAYAJULA, S., GYLFASON, A., COLLINS, L.R., BODENSCHATZ, E. & WARHAFT, Z. 2006 Lagrangian measurements of inertial particle accelerations in grid generated wind tunnel turbulence. *Phys. Rev. Lett.* **97** (14), 144507.

BAKER, L.J., FRANKEL, A., MANI, A. & COLETTI, F. 2017 Coherent clusters of inertial particles in homogeneous turbulence. *J. Fluid Mech.* **833**, 364–398.

BALACHANDAR, S. & EATON, J.K. 2010 Turbulent dispersed multiphase flow. *Annu. Rev. Fluid Mech.* **42**, 111–133.

BALACHANDAR, S., LIU, K. & LAKHOTE, M. 2019 Self-induced velocity correction for improved drag estimation in Euler–Lagrange point-particle simulations. *J. Comput. Phys.* **376**, 160–185.

BEC, J., BIFERALE, L., BOFFETTA, G., CELANI, A., LANOTTE, A., MUSACCIO, S. & TOSCHI, F. 2006 Acceleration statistics of heavy particles in turbulence. *J. Fluid Mech.* **550**, 349–358.

BEC, J., BIFERALE, L., CENCINI, M. & LANOTTE, A.S. 2010 Intermittency in the velocity distribution of heavy particles in turbulence. *J. Fluid Mech.* **646**, 527–536.

BEC, J., HOMANN, H. & RAY, S.S. 2014 Gravity-driven enhancement of heavy particle clustering in turbulent flow. *Phys. Rev. Lett.* **112** (18), 184501.

BERK, T. & COLETTI, F. 2021 Dynamics of small heavy particles in homogeneous turbulence: a Lagrangian experimental study. *J. Fluid Mech.* **917**, A47.

BOSSE, T., KLEISER, L. & MEIBURG, E. 2006 Small particles in homogeneous turbulence: settling velocity enhancement by two-way coupling. *Phys. Fluids* **18** (2), 027102.

BOURGOIN, M. 2015 Turbulent pair dispersion as a ballistic cascade phenomenology. *J. Fluid Mech.* **772**, 678–704.

BRAGG, A.D. & COLLINS, L.R. 2014 New insights from comparing statistical theories for inertial particles in turbulence. I. Spatial distribution of particles. *New J. Phys.* **16** (5), 055013.

BRAGG, A.D., HAMMOND, A.L., DHARIWAL, R. & MENG, H. 2022 Hydrodynamic interactions and extreme particle clustering in turbulence. *J. Fluid Mech.* **933**, A31.

BRANDT, L. & COLETTI, F. 2022 Particle-laden turbulence: progress and perspectives. *Annu. Rev. Fluid Mech.* **54**, 159–189.

CAPECELATRO, J. & DESJARDINS, O. 2013 An Euler–Lagrange strategy for simulating particle-laden flows. *J. Comput. Phys.* **238**, 1–31.

CAPECELATRO, J., DESJARDINS, O. & FOX, R.O. 2014 Numerical study of collisional particle dynamics in cluster-induced turbulence. *J. Fluid Mech.* **747**, R2.

CAPECELATRO, J., DESJARDINS, O. & FOX, R.O. 2018 On the transition between turbulence regimes in particle-laden channel flows. *J. Fluid Mech.* **845**, 499–519.

CARTER, D., PETERSEN, A., AMILI, O. & COLETTI, F. 2016 Generating and controlling homogeneous air turbulence using random jet arrays. *Exp. Fluids* **57** (12), 189.

CARTER, D.W. & COLETTI, F. 2017 Scale-to-scale anisotropy in homogeneous turbulence. *J. Fluid Mech.* **827**, 250–284.

CARTER, D.W. & COLETTI, F. 2018 Small-scale structure and energy transfer in homogeneous turbulence. *J. Fluid Mech.* **854**, 505–543.

CHOUIPPE, A. & UHLMANN, M. 2019 On the influence of forced homogeneous-isotropic turbulence on the settling and clustering of finite-size particles. *Acta Mechanica* **230**, 387–412.

CISSE, M., HOMANN, H. & BEC, J. 2013 Slipping motion of large neutrally buoyant particles in turbulence. *J. Fluid Mech.* **735**, R1.

CLIFT, R., GRACE, J.R. & WEBER, M.E. 2005 *Bubbles, Drops and Particles*. Dover.

COSTA, P., BRANDT, L. & PICANO, F. 2020 Interface-resolved simulations of small inertial particles in turbulent channel flow. *J. Fluid Mech.* **883**, A54.

CSANADY, G.T. 1963 Turbulent diffusion of heavy particles in the atmosphere. *J. Atmos. Sci.* **20** (3), 201–208.

DISCETTI, S. & COLETTI, F. 2018 Volumetriy velocimetry for fluid flows. *Meas. Sci. Technol.* **29** (4), 042001.

DOU, Z., BRAGG, A.D., HAMMOND, A.L., LIANG, Z., COLLINS, L.R. & MENG, H. 2018 Effects of Reynolds number and Stokes number on particle-pair relative velocity in isotropic turbulence: a systematic experimental study. *J. Fluid Mech.* **839**, 271–292.

EATON, J.K. 2009 Two-way coupled turbulence simulations of gas–particle flows using point-particle tracking. *Intl J. Multiphase Flow* **35** (9), 792–800.

EATON, J.K. & FESSLER, J. 1994 Preferential concentration of particles by turbulence. *Intl J. Multiphase Flow* **20**, 169–209.

ELGHOBASHI, S. 1994 On predicting particle-laden turbulent flows. *Appl. Sci. Res.* **52** (4), 309–329.

ELGHOBASHI, S. & TRUESDELL, G.C. 1992 Direct simulation of particle dispersion in decaying isotropic turbulence. *J. Fluid Mech.* **242**, 655–700.

FEVRIER, P., SIMONIN, O. & SQUIRES, K.D. 2005 Partitioning of particle velocities in gas–solid turbulent flows into a continuous field and a spatially uncorrelated random distribution: theoretical formalism and numerical study. *J. Fluid Mech.* **533**, 1–46.

FONG, K.O., AMILI, O. & COLETTI, F. 2019 Velocity and spatial distribution of inertial particles in a turbulent channel flow. *J. Fluid Mech.* **872**, 367–406.

FORNARI, W., PICANO, F. & BRANDT, L. 2016 Sedimentation of finite-size spheres in quiescent and turbulent environments. *J. Fluid Mech.* **788**, 640–669.

FRANKEL, A., POURANSARI, H., COLETTI, F. & MANI, A. 2016 Settling of heated particles in homogeneous turbulence. *J. Fluid Mech.* **792**, 869–893.

GARCIA-VILLALBA, M., KIDANEMARIAM, A.G. & UHLMANN, M. 2012 DNS of vertical plane channel flow with finite-size particles: Voronoï analysis, acceleration statistics and particle-conditioned averaging. *Intl J. Multiphase Flow* **46**, 54–74.

GOOD, G.H., IRELAND, P.J., BEWLEY, G.P., BODENSCHATZ, E., COLLINS, L.R. & WARHAFT, Z. 2014 Settling regimes of inertial particles in turbulence. *J. Fluid Mech.* **759**, R3.

GOTO, S. & VASSILICOS, J.C. 2006 Self-similar clustering of inertial particles and zero-acceleration points in fully developed two-dimensional turbulence. *Phys. Fluids* **18** (11), 115103.

GOTO, S. & VASSILICOS, J.C. 2008 Sweep-stick mechanism of heavy particle clustering in fluid turbulence. *Phys. Rev. Lett.* **100** (5), 054503.

GUALTIERI, P., PICANO, F., SARDINA, G. & CASCIOLA, C.M. 2013 Clustering and turbulence modulation in particle-laden shear flows. *J. Fluid Mech.* **715**, 134–162.

GUALTIERI, P., PICANO, F., SARDINA, G. & CASCIOLA, C.M. 2015 Exact regularized point particle method for multiphase flows in the two-way coupling regime. *J. Fluid Mech.* **773**, 520–561.

GUSTAVSSON, K. & MEHLIG, B. 2016 Statistical models for spatial patterns of heavy particles in turbulence. *Adv. Phys.* **65** (1), 1–57.

GUSTAVSSON, K., VAJEDI, S. & MEHLIG, B. 2014 Clustering of particles falling in a turbulent flow. *Phys. Rev. Lett.* **112**, 214501.

HASSAINI, R. & COLETTI, F. 2022 Scale-to-scale turbulence modification by small settling particles. *J. Fluid Mech.* **949**, A30.

HOLTZER, G.L. & COLLINS, L.R. 2002 Relationship between the intrinsic radial distribution function for an isotropic field of particles and lower-dimensional measurements. *J. Fluid Mech.* **459**, 93–102.

HORWITZ, J. & MANI, A. 2016 Accurate calculation of Stokes drag for point-particle tracking in two-way coupled flows. *J. Comput. Phys.* **318**, 85–109.

HORWITZ, J.A.K. & MANI, A. 2020 Two-way coupled particle–turbulence interaction: effect of numerics and resolution on fluid and particle statistics. *Phys. Rev. Fluids* **5** (10), 104302.

HWANG, W. & EATON, J.K. 2006 Homogeneous and isotropic turbulence modulation by small heavy ($St \sim 50$) particles. *J. Fluid Mech.* **564**, 361–393.

IRELAND, P.J., BRAGG, A.D. & COLLINS, L.R. 2016a The effect of Reynolds number on inertial particle dynamics in isotropic turbulence. Part 1. Simulations without gravitational effects. *J. Fluid Mech.* **796**, 617–658.

IRELAND, P.J., BRAGG, A.D. & COLLINS, L.R. 2016b The effect of Reynolds number on inertial particle dynamics in isotropic turbulence. Part 2. Simulations without gravitational effects. *J. Fluid Mech.* **796**, 659–711.

IRELAND, P.J. & DESJARDINS, O. 2017 Improving particle drag predictions in Euler–Lagrange simulations with two-way coupling. *J. Comput. Phys.* **338**, 405–430.

KOLMOGOROV, A.N. 1941 The local structure of turbulence in incompressible viscous fluid for very large Reynolds numbers. *C. R. Acad. Sci.* **30**, 301–305.

KUERTEN, J.G.M. 2016 Point-particle DNS and LES of particle-laden turbulent flow – a state-of-the-art review. *Flow Turbul. Combust.* **97**, 689–713.

LIN, Z.W., SHAO, X.M., YU, Z.S. & WANG, L.P. 2017 Effects of finite-size heavy particles on the turbulent flows in a square duct. *J. Hydrodyn.* **29** (2), 272–282.

LIU, Y., SHEN, L., ZAMANSKY, R. & COLETTI, F. 2020 Life and death of inertial particle clusters in turbulence. *J. Fluid Mech.* **902**, R1.

LUCCI, F., FERRANTE, A. & ELGHOBASHI, S. 2010 Modulation of isotropic turbulence by particles of Taylor length-scale size. *J. Fluid Mech.* **650**, 5–55.

MAXEY, M.R. 1987 The motion of small spherical particles in a cellular flow field. *Phys. Fluids* **30** (7), 1915–1928.

MEHRABADI, M., HORWITZ, J.A.K., SUBRAMANIAM, S. & MANI, A. 2018 A direct comparison of particle-resolved and point-particle methods in decaying turbulence. *J. Fluid Mech.* **850**, 336–369.

MONCHAUX, R. 2012 Measuring concentration with Voronoï diagrams: the study of possible biases. *New J. Phys.* **14** (9), 095013.

MONCHAUX, R., BOURGOIN, M. & CARTELLIER, A. 2010 Preferential concentration of heavy particles: a Voronoï analysis. *Phys. Fluids* **22** (12), 103304.

MONCHAUX, R., BOURGOIN, M. & CARTELLIER, A. 2012 Analyzing preferential concentration and clustering of inertial particles in turbulence. *Intl J. Multiphase Flow* **40**, 1–18.

MONCHAUX, R. & DEJOAN, A. 2017 Settling velocity and preferential concentration of heavy particles under two-way coupling effects in homogeneous turbulence. *Phys. Rev. Fluids* **2** (10), 104302.

NIELSEN, P. 1993 Turbulence effects on the settling of suspended particles. *J. Sedim. Res.* **63** (5), 835–838.

PETERSEN, A.J., BAKER, L.J. & COLETTI, F. 2019 Experimental study of inertial particles clustering and settling in homogeneous turbulence. *J. Fluid Mech.* **864**, 925–970.

POELMA, C. & OOMS, G. 2006 Particle–turbulence interaction in a homogeneous, isotropic turbulent suspension. *Appl. Mech. Rev.* **59**, 78–90.

POELMA, C., WESTERWEEL, J. & OOMS, G. 2007 Particle–fluid interactions in grid-generated turbulence. *J. Fluid Mech.* **589**, 315–351.

QURESHI, N.M., ARRIETA, U., BAUDET, C., CARTELLIER, A., GAGNE, Y. & BOURGOIN, M. 2008 Acceleration statistics of inertial particles in turbulent flow. *Eur. Phys. J.* B **66**, 531–536.

QURESHI, N.M., BOURGOIN, M., BAUDET, C., CARTELLIER, A. & GAGNE, Y. 2007 Turbulent transport of material particles: an experimental study of finite size effects. *Phys. Rev. Lett.* **99** (18), 184502.

READE, W.C. & COLLINS, L.R. 2000 Effect of preferential concentration on turbulent collision rates. *Phys. Fluids* **12** (10), 2530–2540.

RICHTER, D.H. & SULLIVAN, P.P. 2014 Modification of near-wall coherent structures by inertial particles. *Phys. Fluids* **26** (10), 103304.

ROSA, B., KOPEĆ, S., ABABAEI, A. & POZORSKI, J. 2022 Collision statistics and settling velocity of inertial particles in homogeneous turbulence from high-resolution DNS under two-way momentum coupling. *Intl J. Multiphase Flow* **148**, 103906.

ROSA, B., POZORSKI, J. & WANG, L.-P. 2020 Effects of turbulence modulation and gravity on particle collision statistics. *Intl J. Multiphase Flow* **129**, 103334.

SAITO, I., WATANABE, T. & GOTOH, T. 2019 A new time scale for turbulence modulation by particles. *J. Fluid Mech.* **880**, R6.

SCHNEIDERS, L., MEINKE, M. & SCHRÖDER, W. 2017 Direct particle–fluid simulation of Kolmogorov-length-scale size particles in decaying isotropic turbulence. *J. Fluid Mech.* **819**, 188–227.

SCHRÖDER, A. & SCHANZ, D. 2023 3D Lagrangian particle tracking in fluid mechanics. *Annu. Rev. Fluid Mech.* **55**, 511–540.

SQUIRES, K.D. & EATON, J.K. 1991*a* Measurements of particles dispersion obtained from direct numerical simulations of isotropic turbulence. *J. Fluid Mech.* **226**, 1–35.

SQUIRES, K.D. & EATON, J.K. 1991*b* Preferential concentration of particles by turbulence. *Phys. Fluids* A **3** (5), 1169–1178.

SUMBEKOVA, S., CARTELLIER, A., ALISEDA, A. & BOURGOIN, M. 2017 Preferential concentration of inertial sub-Kolmogorov particles: the roles of mass loading of particles, Stokes numbers, and Reynolds numbers. *Phys. Rev. Fluids* **2**, 024302.

SUNDARAM, S. & COLLINS, L.R. 1997 Collision statistics in an isotropic particle-laden turbulent suspension. Part 1. Direct numerical simulations. *J. Fluid Mech.* **335**, 75–109.

TANAKA, T. & EATON, J.K. 2010 Sub-Kolmogorov resolution particle image velocimetry measurements of particle-laden forced turbulence. *J. Fluid Mech.* **643**, 177–206.

TENNETI, S. & SUBRAMANIAM, S. 2014 Particle-resolved direct numerical simulation for gas–solid flow model development. *Annu. Rev. Fluid Mech.* **46**, 199–230.

TOM, J. & BRAGG, A.D. 2019 Multiscale preferential sweeping of particles settling in turbulence. *J. Fluid Mech.* **871**, 244–270.

TOM, J., CARBONE, M. & BRAGG, A.D. 2022 How two-way coupling modifies the multiscale preferential sweeping mechanism. *J. Fluid Mech.* **947**, A7.

UHLMANN, M. & CHOUIPPE, A. 2017 Clustering and preferential concentration of finite-size particles in forced homogeneous-isotropic turbulence. *J. Fluid Mech.* **812**, 991–1023.

UHLMANN, M. & DOYCHEV, T. 2014 Sedimentation of a dilute suspension of rigid spheres at intermediate Galileo numbers: the effect of clustering upon the particle motion. *J. Fluid Mech.* **752**, 310–348.

WANG, G., FONG, K.O., COLETTI, F., CAPECELATRO, J. & RICHTER, D.H. 2019 Inertial particle velocity and distribution in vertical turbulent channel flow: a numerical and experimental comparison. *Intl J. Multiphase Flow* **120**, 103105.

WANG, L.P. & MAXEY, M.R. 1993 Settling velocity and concentration distribution of heavy particles in homogeneous isotropic turbulence. *J. Fluid Mech.* **256**, 27–68.

WANG, L.P. & STOCK, D.E. 1993 Dispersion of heavy particles by turbulent motion. *J. Atmos. Sci.* **50** (13), 1897–1913.

WILKINSON, M. & MEHLIG, B. 2005 Caustics in turbulent aerosols. *Europhys. Lett.* **71** (2), 186.

YANG, T.S. & SHY, S.S. 2005 Two-way interaction between solid particles and homogeneous air turbulence: particle settling rate and turbulence modification measurements. *J. Fluid Mech.* **526**, 171–216.

YOSHIMOTO, H. & GOTO, S. 2007 Self-similar clustering of inertial particles in homogeneous turbulence. *J. Fluid Mech.* **577**, 275–286.

ZHAO, L., ANDERSSON, H.I. & GILLISSEN, J.J. 2013 Interphasial energy transfer and particle dissipation in particle-laden wall turbulence. *J. Fluid Mech.* **715**, 32–59.

ZÜRNER, T., TOUPOINT, C., DE SOUZA, D., MEZOUANE, D. & MONCHAUX, R. 2023 Settling of localized particle plumes in a quiescent water tank. *Phys. Rev. Fluids* **8** (2), 024301.